

Development and Design of a 340 GHz Photomixer Source

Biddut Banik, Josip Vukusic, Syed Mahmudur Rahman, Henrik Sunnerud and Jan Stake

Abstract— We present the design of an InGaAlAs/InP uni-traveling-carrier photo-diode (UTC-PD) at mm-wave frequencies up to 340 GHz. The photo diode epitaxy is optimized using a quasi-3D software implementing the hydrodynamic semiconductor equations, for which an output power of 3 mW at 340 GHz was simulated. An equivalent circuit of the UTC-PD has been fitted to experimental S_{11} measurements up to 67 GHz. Finally, an optimized antenna coupled UTC-PD with choke filter has been designed. This MMIC circuit is intended for photomixing, with output power at 340 GHz.

Index Terms— Photomixer, terahertz source, uni-traveling carrier photo-diode

I. INTRODUCTION

THE increasing demand for sources in the THz frequency regime has prompted a numerous number of electrical and optical schemes for the generation of sub-mm waves. Photomixing, being one of these schemes, relies on the nonlinear mixing of two closely spaced laser wavelengths generating a beat oscillation at the difference frequency, as exemplified in Fig.1. One of the benefits of using this method is the wide tunability of the output frequency. The 350 GHz [1] band has interesting applications for remote sensing of atmospheric gases, which needs a local oscillator (LO) for sensitive detection. By using a laser fed LO source the signal can be easily distributed by fiber optics and can be used in antenna networks for instance.

In the recent years, there has been an increasing interest in the Uni-Traveling-Carrier Photodiode (UTC-PD) for photomixing, photo receivers, microwave and mm-wave generation, fiber-optic communication systems and wireless communications. UTC-PDs offer several advantages over PIN-PDs. A UTC-PD uses only electrons as the active carriers and hole transport does not directly affect the diode response and output saturation. UTC-PDs have become very promising by demonstrating output powers of 20 mW at 100 GHz [2]

Manuscript received June 21, 2007. This work was supported by the Swedish Foundation for Strategic Research (SSF).

Biddut Banik, Josip Vukusic, Syed Mahmudur Rahman and Jan Stake are with the Physical Electronics Laboratory, Dept. of Microtechnology and Nanoscience, Chalmers University of Technology; SE-41296, Göteborg, Sweden (e-mail: biddut.banik@mc2.chalmers.se).

Henrik Sunnerud is with the Photonics Laboratory, Dept. of Microtechnology and Nanoscience, Chalmers University of Technology; SE-41296, Göteborg, Sweden (e-mail: sunnerud@chalmers.se).

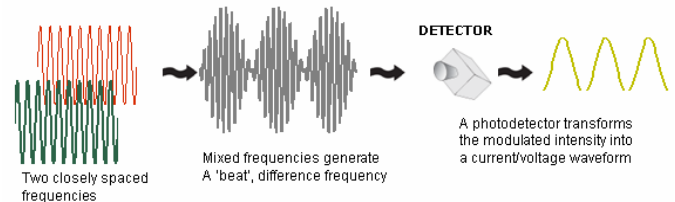


Fig.1. By shifting the laser wavelength slightly we can achieve wide tunability of our electrical output

and 25 μ W at 1 THz [3].

We report our research results based on the InGaAlAs/InP uni-traveling-carrier photo-diode (UTC-PD) at lower frequencies (<60 GHz) extending up to 340 GHz. Our research goal encompasses realization of compact and tunable THz sources by photomixing and integration of the photomixer with antennas.

II. UNI-TRAVELING CARRIER PHOTO-DIODE

A. Working Principle

Electron-hole pairs are generated when the light is absorbed in a photo diode. For the conventional PIN-PD this occurs in the undoped, intrinsic region. This results in an approximately equal length of transport for both holes and electrons. Because of the significantly larger mass of the holes these limit the speed of the device. In a UTC-PD on the other hand, the light is absorbed in the p-doped region thereby significantly shortening the distance to the p-contact for the holes. In this way we also avoid the build-up of holes that would at some point screen the acceleration field normally present in the device. Fig.2 shows a comparison between the operational principles of the PIN-PD and the UTC-PD. In the conventional PIN-PD, under a high-excitation condition the band profile changes as photo-generated carriers are accumulated in the absorption layer. This in turn decreases the electric field and drastically reduces the carrier velocity and results in output current saturation. In the case of the UTC-PD, the space charge consists of only electrons whose velocity at overshoot is much higher than that of holes, even for the decreased electric field, and thus postpones current saturation. In UTC-PDs, high electron mobility in the depletion layer can be maintained at a relatively low electric field or even with the built-in field of the p - n junction. This enables high-speed operation of the UTC-PD without applying any bias voltage. The device thereby offers higher operation current and lower

operation voltage [4].

We can see from Fig. 2 that UTC-PDs have separate absorption and depletion regions. The absorption layer and the depletion layer thicknesses in the UTC-PD structure can therefore be independently designed. This means that a very thin absorption layer can be used for higher bandwidth without sacrificing the RC charging time. On the other hand, in the PIN-PD the RC charging time becomes significantly larger when the absorption layer thickness is excessively reduced to decrease the carrier transit time.

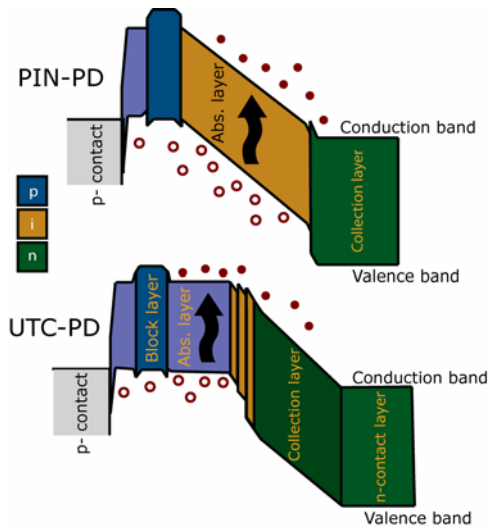


Fig.2. Schematic band diagrams of a PIN-PD and an UTC-PD [5]

This work features InGaAlAs/InP UTC-PD devices for which InGaAs is the absorbant and 1.55 μm is the operating wavelength. By using this standard telecommunications wavelength we have a wide spectrum of relatively inexpensive, high performance equipment at our disposal.

B. Device Fabrication

The fabrication of the InGaAlAs/InP UTC-PD's is initiated by growth of the material layering by our in house molecular beam epitaxy (MBE) system. To fabricate the devices standard III-V processing techniques are used. This includes photolithography UV/DUV, E-beam evaporation, contact annealing, wet etching, dry etching and electroplating. To facilitate efficient light collection by the bottom illuminated devices the substrate is thinned by lapping and polishing. This is followed by Si_3N_4 anti-reflection coating. Fig. 3 shows SEM photograph of two fabricated UTC-PDs of different sizes with air-bridges.

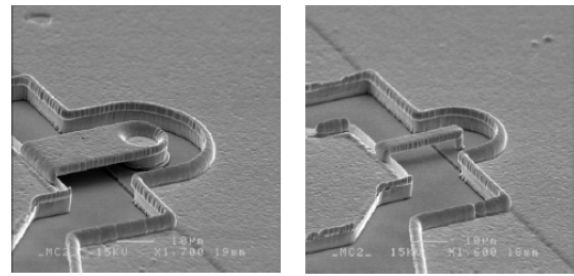


Fig.3. SEM photograph of the fabricated UTC-PDs with a detector diameter of 20 μm and 3 μm respectively.

C. Device characterization

Fabricated devices with 8-17 micron diameters and 220 nm absorption layer widths were characterized. These devices had a 50 Ohm coplanar waveguide leading up to the device itself. The photo-diodes were excited by 1 ps pulses with a 50 MHz repetition frequency. By simultaneously probing the open end of the waveguide using a 70 GHz sampling oscilloscope we were able to estimate the 3-dB bandwidth of the UTC-PDs. The upper graph of Fig. 4 shows an example of the sampled impulse response for an 8 micron device. Because of the frequency dependent losses from the bias-T, cables and probes a significantly lower 3-dB bandwidth was measured. By compensating for the influence of the measurement setup, as seen in the lower graph of Fig. 4, we arrived at an expected 3-dB bandwidth of 60 GHz for these devices.

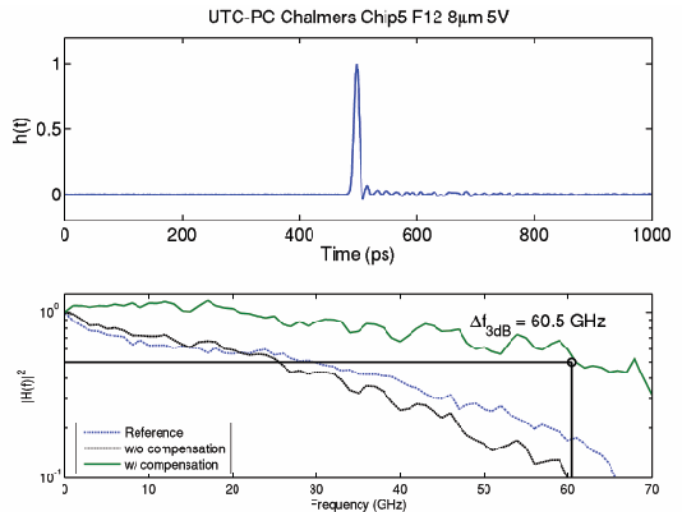


Fig.4. (upper) impulse response from an 8 mm UTC-PD. (lower) Fourier transform of the impulse response with the bandwidth limitations of the measurement setup included

Fig. 5 shows the 3-dB bandwidth for different power injection levels. We can see that the detector response saturates at pulse energies above 1 pJ. Also, we can note that 10 V reverse bias is more successful in sweeping the large number of electrons through the device. As discussed earlier, the large number of generated carriers distort the acceleration field. But by applying a high external voltage we

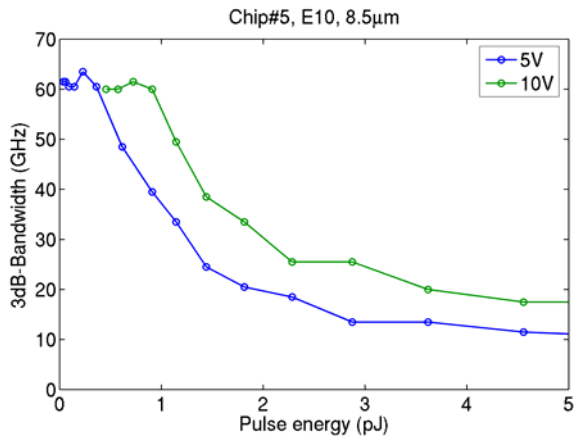


Fig.5. 3-dB bandwidth versus input pulse energy of an 8 micron device with a 220 nm absorption layer

counteract this distortion and the onset of the saturation can be postponed.

D. Equivalent Circuit

In order to understand the impedance behavior of the photo detector we have compared measured s-parameters with an equivalent circuit model. This will allow us to estimate the device impedance when scaling down the detector area for higher frequencies.

In principle, the equivalent circuit of a UTC-PD can be

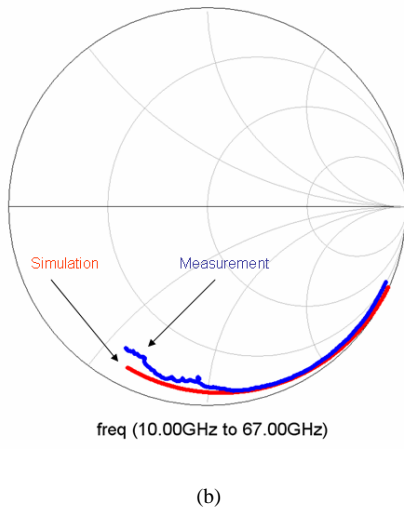
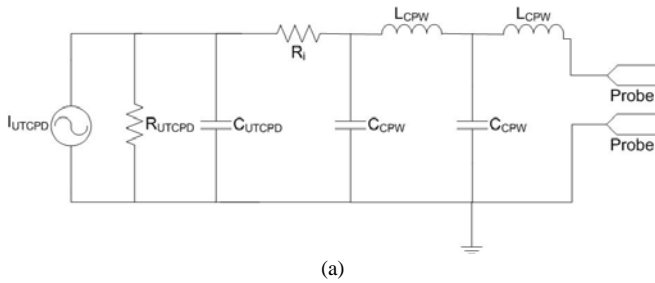


Fig.6. (a) Equivalent circuit of the UTC-PD (b) simulation and measurement results (S_{11}).

realized as a current source I_{UTCPD} in parallel with a very high resistance R_{UTCPD} and capacitance C_{UTCPD} . The fabricated UTC-PD devices have a short strip of coplanar waveguide (CPW) leading up to them to accommodate the measurement probes. The equivalent circuit for UTC-PD and CPW, shown in Fig. 6 (a), is modeled in Advanced Design System (ADS). The CPW is modeled as a cascade of series inductance L_{CPW} and shunt capacitance C_{CPW} . Fig. 6 (b) shows the S_{11} plot attained by simulation and measurement from 10 GHz to 67 GHz.

III. EPITAXIAL MODELING

To optimize the UTC-PDC epitaxial layering for the task at hand, we implemented a quasi-3D model using a commercial TCAD software [6]. Fig. 7 shows the graphical user interface describing the epitaxial layering of the device.

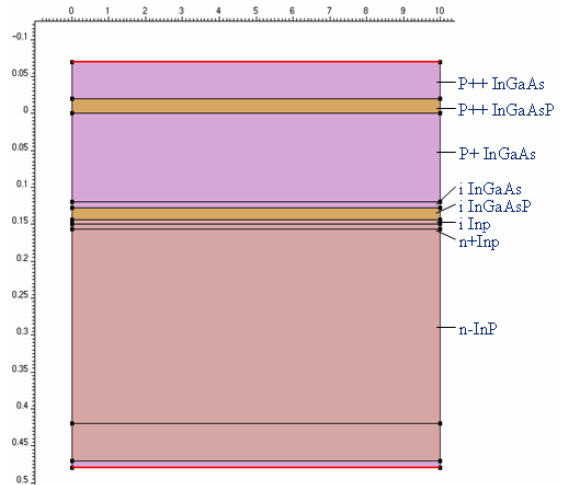
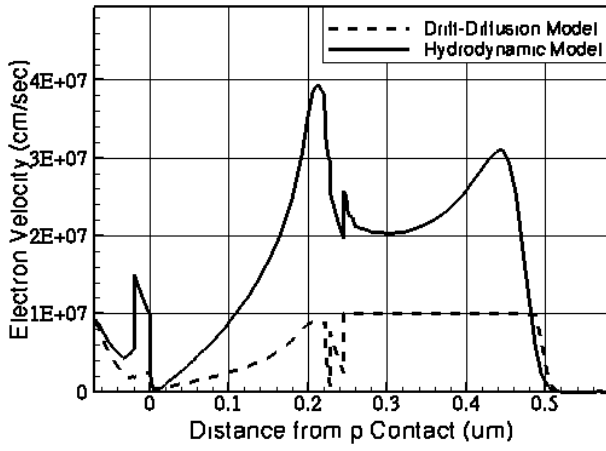


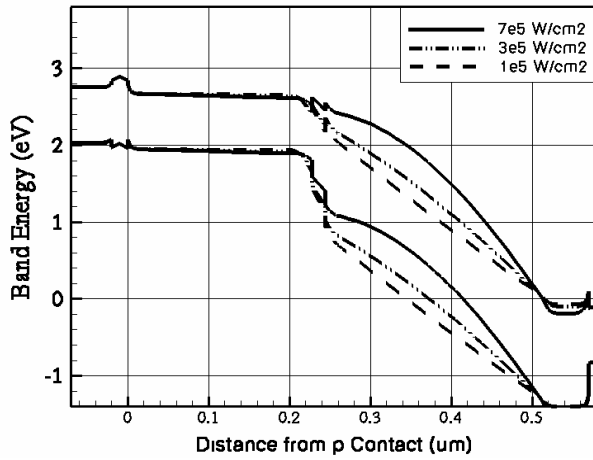
Fig.7. Graphical user interface of the TCAD software with the layer compositions marked

These calculations use the hydrodynamic model to model the carrier transport through the photo-detector. In this way we take into account the velocity overshoot in the device. Fig. 8 (a) shows the difference in electron velocity between the conventional drift diffusion (DD) and the hydrodynamic (HD) model. Since the carrier transport in the UTC-PD is predominantly governed by electrons the significant discrepancy between the DD and HD model will influence the simulation results. Fig. 8 (b) shows the energy band diagram under different optical injection levels. We can see that above some injection level the carrier accumulation impairs the acceleration field in the collector region and thereby saturates the detector response.

This is also evident in Fig. 9 (a) in which the detector responsivity has been plotted against different optical input powers. We can see that at some point saturation effects limit the amount of power that the UTC-PD can handle. Note also the difference between the DD and the HD model. Since the DD model doesn't include velocity overshoot effects it clearly underestimates the power handling of the device.

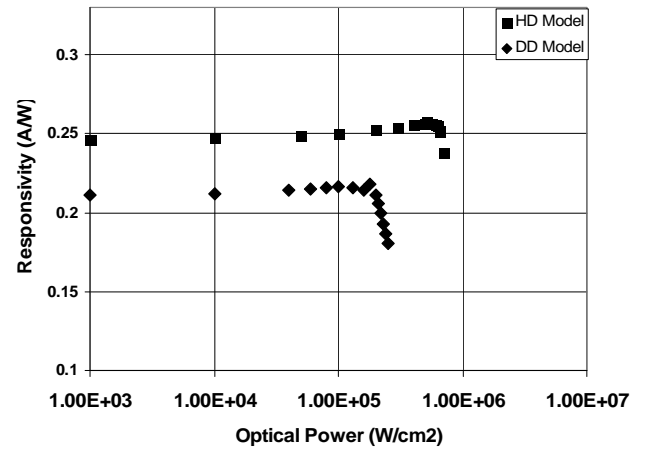


(a)

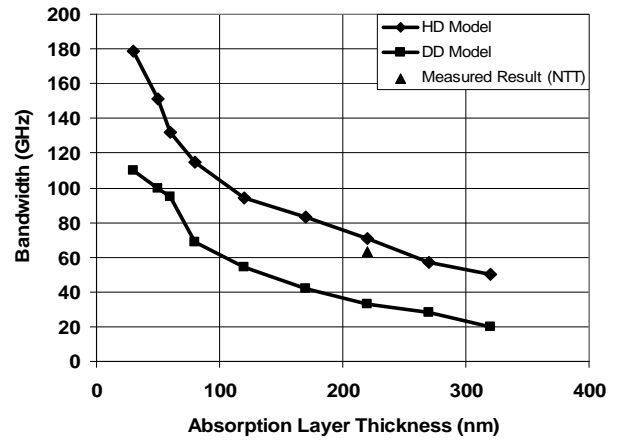


(b)

Fig.8. (a) Electron velocity distribution across the UTC-PD (b) Energy band-diagram for different optical injection levels calculated using the HD model



(a)



(b)

Fig.9. (a) Responsivity at different optical input powers (b) Bandwidth for different absorption layer thicknesses

Fig. 9 (b) shows a comparison between the DD and the HD model bandwidths for different absorption layer thicknesses. Again we can see that the bandwidth is underestimated by the DD model because of the inability to predict the velocity overshoot. An experimental result has also been included in the graph for comparison at 220 nm absorption layer thickness.

IV. LAYER OPTIMIZATION EXAMPLE

Our goal is to design and optimize a 340 GHz photomixer. So we can therefore use the implemented software to change layer thicknesses of our epitaxy to maximize the output power. In this case we have chosen to vary the collection and absorption layer thickness. The positions of these layers are shown in Fig. 10. An optical pulse train with 340 GHz frequency and at different power levels was fed into the device to mimic photomixing. Fig. 11 (a) shows the resulting output power when varying the absorption layer thickness for a fixed (263 nm) collection layer thickness. We can see that a thickness of ~38 nm was optimum. By keeping the absorption layer constant (38 nm) we then varied the collection layer thickness. This is presented in Fig. 11 (b), where we can see

that the optimum collection layer thickness was 140 nm.

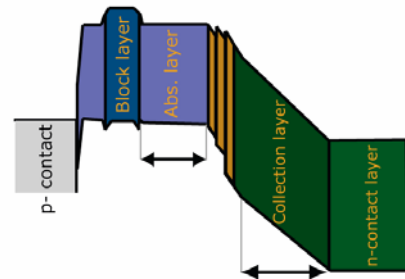


Fig.10. Simulations varying the absorption and collection layer widths

The trade off in this case is between long carrier transit time for a thick collection layer and the high capacitance (RC-constant) for a thin collection layer. We can note that the maximum output power is slightly above 3 mW. In these calculations we have not included any losses in the outcoupling of the radiation. Also, this optimization was done without any thermal analysis, which may limit the manageable input power.

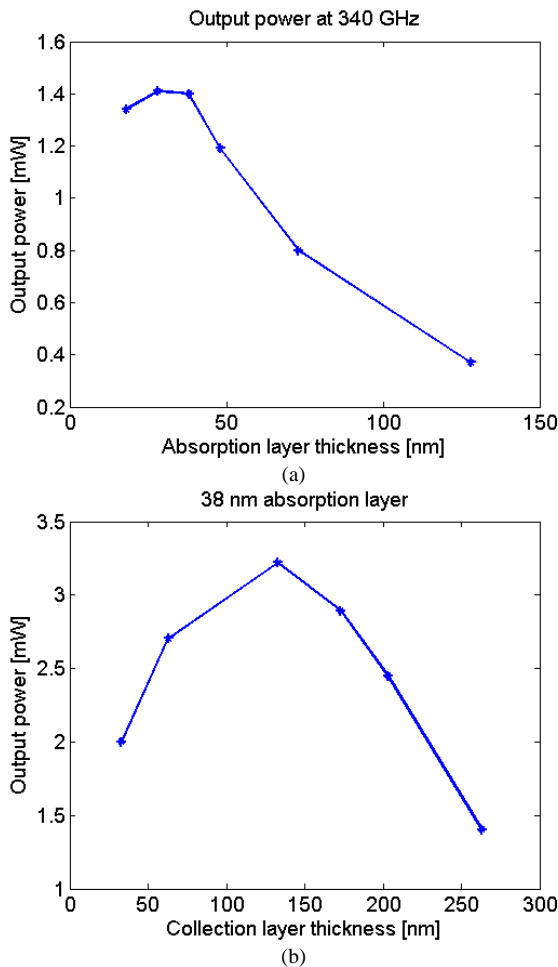


Fig.11. (a) Optimization of the absorption layer thickness s (b) Optimization of the collection layer thickness

V. ANTENNA DESIGN

Due to the benefits of THz technology in various applications such as security and imaging systems, photomixing with UTC-PDs have proven to be an attractive solution for THz generation. A convenient approach for the realization of a THz emitter is to integrate the photo detector with an antenna.

As shown in [7], the THz output power from a photomixer is proportional to the antenna impedance. For UTC-PD-antenna integration, different types of antennas such as bowtie, log-spiral and log-periodic antenna have been reported. However, the impedance of those broadband antennas is relatively low [8-11]. Resonant antennas such as dipole and slot antennae offer relatively high impedance at the resonant frequency [11, 12]. Photomixing with resonant twin-dipole and twin-slot antennae has also been reported [13].

Twin-dipole antennas provide symmetric near-Gaussian beam pattern. Another advantage of twin-dipole antennas is that the high directive gain reduces the reflection loss at the surface of a silicon substrate lens. Twin-dipole antennas offer the flexibility of inductance tuning by adjusting the length of the transmission line connecting the photoconductive gap and the antenna. This feature enables us to cancel the capacitance

of the photoconductive gap and thereby reducing the bandwidth limiting RC-constant

Compared to microstrip lines and coplanar waveguides, coplanar stripline (CPS) provides higher characteristics impedance [14] and hence suitable for designing antennas with higher impedance. Our goal was to design an antenna for the UTC-PD which can be monolithically integrated, offers higher antenna impedance and thus provides higher power.

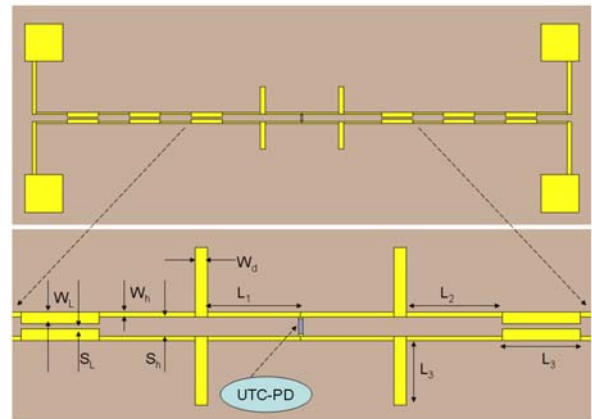


Fig.12. 340 GHz UTC-PD antenna with choke filter and biaspads

Therefore, a twin-dipole CPS antenna on 150 μm thick InP substrate with gold conductor (2 μm thick) was designed having choke filters and biaspads [15]. Fig.12 shows the center-fed twin-dipole antenna and the corresponding design parameters. In the design, the dimensions were $W_h = 5 \mu\text{m}$, $S_h = 20 \mu\text{m}$. At first the Hi Z – Low Z choke filter was designed and optimized in Ansoft HFSS by varying L_3 .

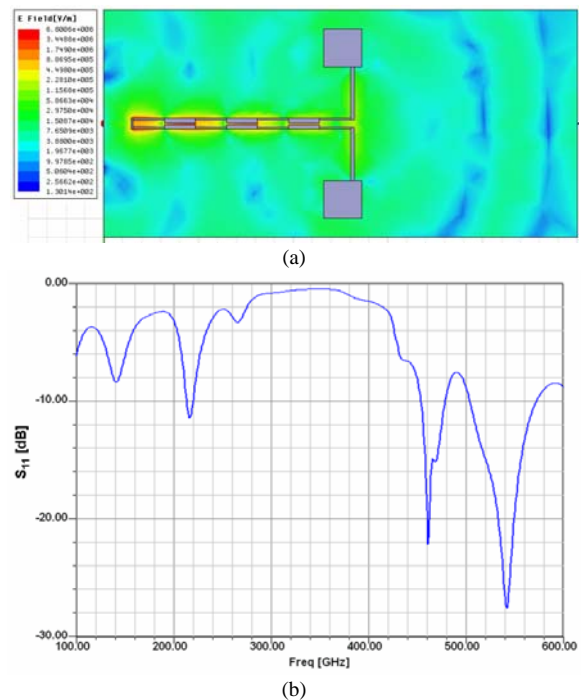


Fig.13. (a) E-field distribution through Hi Z – Low Z steps of the choke filter (b) return loss of the choke filter, resonance at 340 GHz

Fig.13 (a) illustrates the E-field distribution through the Hi Z- Low Z choke filter. Fig.13 (b) shows the return loss of the choke filter. After optimization, a pronounced resonance is observed at 340 GHz where the real part of the input impedance becomes very high and effectively acts as an open circuit. Therefore, at 340 GHz the choke filter provides very high return loss, as can be seen in Fig. 13 (b).

The UTC-PD antenna was then optimized to attain higher input impedance at 340 GHz by varying W_d , L_1 , L_2 and L_3 . Fig. 14 (a) illustrates the E-field distribution through the antenna. Fig. 14 (b) shows the input impedance of the antenna and a pronounced resonance is observed at 340 GHz.

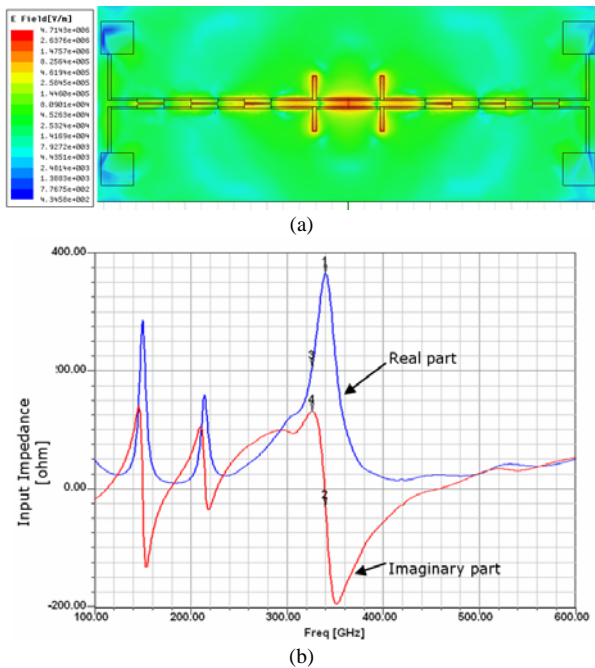


Fig.14. (a) E-field distribution through the twin-dipole antenna (b) Input impedance of the antenna, resonance at 340 GHz

The optimized antenna design, hence, will enable us to eradicate the RC limitation that arises from UTC-PD capacitance. This capacitance can be extracted from the equivalent circuit fit of the s-parameter measurements. The high input impedance of the antennae will maximize the THz output power from the photomixer.

VI. CONCLUSION

We have presented experimental results on UTC-PDs for frequencies up to 67 GHz. This included impulse response and S-parameter measurements. An equivalent circuit was fitted to these results. This was followed by a design methodology for optimizing the output power from a UTC-PD at 340 GHz. The design of the epitaxial layering showed the possibility for ~3 mW of output power. After a short discussion of antenna alternatives the twin-dipole antenna was chosen as the most suitable to integrate with the UTC-PD. The layout of the antenna was then designed to accommodate UTC-PD biasing and optimal impedance matching.

REFERENCES

- [1] H. Smith, R. Hills, S. Withington, J. Richer, J. Leech, R. Williamson, H. Gibson, R. Dace, B. Barker, R. Baldwin, H. Stevenson, P. Doherty, D. Molloy, V. Quy, C. Lush, S. Hales, B. Dent, I. Pain, B. Wall, P. Hastings, B. Graham, T. Baillie, K. Laidlaw, R. Bennett, I. Laidlaw, W. Duncan, M. Ellis, R. Redman, B. Wooff, K. Yeung, J. Fitzsimmons, L. Avery, D. Derald, D. Josephson, A. Anthony, R. Atwal, T. Chylek, D. Shutt, P. Friberg, N. Rees, R. Philips, M. Kroug, T. Klapwijk, T. Zijlstra, and P. G. Ananthasubramanian, "HARP-B: A 350GHz 16-element focal plane array for the James Clerk Maxwell telescope," *Proceedings of SPIE - The International Society for Optical Engineering*, vol. 4855, pp. 338-348, 2002.
- [2] H. Ito, T. Nagatsuma, A. Hirata, T. Minotani, A. Sasaki, Y. Hirota, and T. Ishibashi, "High-power photonic millimetre wave generation at 100 GHz using matching-circuit-integrated uni-travelling-carrier photodiodes," *Optoelectronics, IEE Proceedings*, vol. 150, pp. 138-142, 2003.
- [3] C. C. Renaud, M. Robertson, D. Rogers, R. Firth, P. J. Cannard, R. Moore, and A. J. Seeds, "A high responsivity, broadband waveguide uni-travelling carrier photodiode," *Electronics Letters*, vol. 40, pp. 1297-8, 2004.
- [4] H. Ito, S. Kodama, Y. Muramoto, T. Furuta, T. Nagatsuma, and T. Ishibashi, "High-speed and high-output InP-InGaAs untraveling-carrier photodiodes," *IEEE Journal of Selected Topics in Quantum Electronics*, vol. 10, pp. 709-27, 2004.
- [5] T. Ishibashi, T. Furuta, H. Fushimi, S. Kodama, H. Ito, T. Nagatsuma, N. Shimizu, and Y. Miyamoto, "InP/InGaAs untraveling-carrier photodiodes," *IEICE Transactions on Electronics*, vol. E83-C, pp. 938-49, 2000.
- [6] www.synopsys.com.
- [7] M. Tani, O. Morikawa, S. Matsuura, and M. Hangyo, "Generation of terahertz radiation by photomixing with dual- and multiple-mode lasers," *Semiconductor Science and Technology*, vol. 20, pp. 151-63, 2005.
- [8] E. R. Brown, K. A. McIntosh, K. B. Nichols, and C. L. Dennis, "Photomixing up to 3.8 THz in low-temperature-grown GaAs," *Applied Physics Letters*, vol. 66, pp. 285-7, 1995.
- [9] K. A. McIntosh, E. R. Brown, K. B. Nichols, O. B. McMahon, W. F. Dinatale, and T. M. Lyszczarz, "Terahertz photomixing with diode lasers in low-temperature-grown GaAs," *Applied Physics Letters*, vol. 67, pp. 3844-6, 1995.
- [10] S. Verghese, K. A. McIntosh, and E. R. Brown, "Highly tunable fiber-coupled photomixers with coherent terahertz output power," *IEEE Transactions on Microwave Theory and Techniques*, vol. 45, pp. 1301-9, 1997.
- [11] I. S. Gregory, C. Baker, W. R. Tribe, I. V. Bradley, M. J. Evans, E. H. Linfield, A. G. Davies, and M. Missous, "Optimization of photomixers and antennas for continuous-wave terahertz emission," *IEEE Journal of Quantum Electronics*, vol. 41, pp. 717-728, 2005.
- [12] I. S. Gregory, W. R. Tribe, B. E. Cole, M. J. Evans, E. H. Linfield, A. G. Davies, and M. Missous, "Resonant dipole antennas for continuous-wave terahertz photomixers," *Applied Physics Letters*, vol. 85, pp. 1622-4, 2004.
- [13] S. M. Duffy, S. Verghese, A. McIntosh, A. Jackson, A. C. Gossard, and S. Matsuura, "Accurate modeling of dual dipole and slot elements used with photomixers for coherent terahertz output power," *IEEE Transactions on Microwave Theory and Techniques*, vol. 49, pp. 1032-8, 2001.
- [14] D. Zhengwei, G. Ke, J. S. Fu, F. Zhenghe, and G. Baoxin, "CAD models for asymmetrical, elliptical, cylindrical, and elliptical cone coplanar strip lines," *IEEE Transactions on Microwave Theory and Techniques*, vol. 48, pp. 312-16, 2000.
- [15] H. Ito, F. Nakajima, T. Furuta, and T. Ishibashi, "Continuous THz-wave generation using antenna-integrated uni-travelling-carrier photodiodes," *Semiconductor Science and Technology*, vol. 20, pp. 191-8, 2005.